BIOMIMETICS

Embodying soft robots with octopus-inspired hierarchical suction intelligence

Tianqi Yue[1,2,3], Chenghua Lu[1,3], Kailuan Tang[4], Qiukai Qi[1,3], Zhenyu Lu[3,5], Loong Yi Lee[1,3], Hermes Bloomfield-Gadêlha[1,3], Jonathan Rossiter[1,3]*

Octopuses exploit an efficient neuromuscular hierarchy to achieve complex dexterous body manipulation, integrating sensor-rich suckers, in-arm embodied computation, and centralized higher-level reasoning. Here, we take inspiration from the hierarchical intelligence of the octopus and demonstrate how, by exploiting the fluidic energy and information capacity of simple suction cups, soft computational elements, and soft actuators, we can mimic key aspects of the neuromuscular structure of the octopus in soft robotic systems. The presented suction intelligence works at two levels: By coupling suction flow with local fluidic circuitry, soft robots can achieve octopus-like low-level embodied intelligence, including gently grasping delicate objects, adaptive curling, and encapsulating objects of unknown geometries, and by decoding the pressure response from a suction cup, robots can achieve multimodal high-level perception, including contact detection, classification of an environmental medium and surface roughness, and prediction of an interactive pulling force. As in octopuses, suction intelligence executes most of its computation within lower-level local fluidic circuitries, and minimum information is transmitted to the high-level decision-making of the "brain." This development provides insights into octopus-inspired machine intelligence through low-cost, simple, and easy-to-integrate methods. The presented suction intelligence can be readily integrated into fluidic-driven soft robots to enhance their intelligence and reduce their computational requirement and can be applied widely, from industrial object handling and robotic manufacturing to robot-assisted harvesting and interventional health care.

INTRODUCTION

Many studies have suggested that octopuses use a hierarchical system of neurons and muscles to achieve their sophisticated movements and physical intelligence (*1*, *2*). The central brain is reserved for higher-level reasoning, with basic movement and feedback control executed within the lower-level "arm brain." This devolved intelligence is coordinated by local brachial ganglia within the arms, which have ~60% of the total neurons in the octopus (*3*). The sucker organ is critical for realizing lower-level intelligence in the integrated brachial system (*3*–*8*). Receptors (*9*, *10*) in the rim of the sucker acquire rich information, in the form of neural signals (*6*), when the sucker is physically interacting with the environment, for example, contacting a surface. Local neuromuscular networks, formed by coupled sucker and brachial ganglia and muscles, regulate the lower-level autonomous behavior, whereas the brain is reserved for higher-level decision-making such as initiating and terminating actions (*1*, *3*). By distributing intelligence throughout its body, the information bandwidth to and from the brain is notably reduced, and the octopus thus requires only a minimal axial nerve cord for brain-body communication (*5*). The suckers and arms, as versatile tools for simultaneous adhesion, embodied intelligence, and perception, greatly simplify the total neural structure and lower the computation requirement of the central brain.

The devolved intelligence of the octopus has inspired the design of robots. Exploring octopus-like behavior with suckers, Xie *et al.* presented a simplified control model and used suction cup deformation signals as tactile feedback to enhance motion control (*11*). However, the hardware system was complex, and embodied intelligence was not shown. Strain sensors have been embedded in the disc of the suction cup to detect interactive conditions at the contacting surface (*11*–*13*), mimicking the proprioception of octopus suckers (*4*, *14*). However, the integration of strain sensors into suction cups is nontrivial and limits practical applications. Alternatively, suction conditions can be monitored by fluid-based sensing, for example, by monitoring suction pressure (*15*–*19*). In addition, preprogrammed integrated fluidic circuits offer a path for robots to achieve embodied intelligence (*20*–*27*); however, these systems have not demonstrated the multiple functionalities of octopus suckers and the distributed hierarchy of the octopus neural system. Although suction cups are often used as simple supplementary adhesion tools in robotic systems (*28*–*30*), octopus-like hierarchical systems that integrate suction adhesion, embodied intelligence, and multimodal perception remain largely unexplored.

In this work, we demonstrate that, by incorporating simple suction cups into fluidic-driven soft circuits, robots can establish an octopus-like hierarchical and distributed neuromuscular system and mimic the integrated suction adhesion, embodied intelligence, and multimodal perception of the octopus. We first introduce a suction-based embodied intelligence strategy based on the local integration of sensing and control within the robot body, which enables it to achieve octopus-like lower-level autonomy, including grasping weakly supported delicate objects and sucking and curling around unknown objects. We then demonstrate a suction-based multimodal sensing strategy, which is achieved by a simple signal classifier and enables the robot to perceive multiple environmental conditions, including contact, fluidic viscosity, surface roughness, and pulling force. Last, we demonstrate the fusion of the proposed

[1]School of Engineering Mathematics and Technology, University of Bristol, Bristol, UK. [2]School of Automation and Intelligent Manufacturing, Southern University of Science and Technology, Shenzhen, China. [3]Bristol Robotics Laboratory, Bristol, UK. [4]Department of Mechanical and Energy Engineering, Southern University of Science and Technology, Shenzhen, China. [5]Faculty of Environment and Technology, University of the West of England, Bristol, UK.
*Corresponding author. Email: jonathan.rossiter@bristol.ac.uk

suction-based embodied intelligence and multimodal perception strategies and thereby achieve integrated adhesion, embodied intelligence, and multimodal perception in a simple suction gripper with a hierarchical neural structure. Once it receives an activation signal from the higher-level controller, the gripper can autonomously execute the extend-suck-retract action while simultaneously detecting and measuring object properties.

RESULTS

Bioinspiration of octopus suction intelligence

An octopus has 40 million neurons in each arm, used for lower-level sensing and autonomy, and 180 million neurons in the central brain used for higher-level perceptual processing and decision-making (*5*, *10*). Despite the large numbers of neurons distributed throughout the body, only 32,000 efferents and 140,000 afferents form the axial cord, which communicates between the arms and the central brain (*3*, *31*) [Fig. 1A (i)]. This physiology is only possible if the devolved organs (arms) can undertake autonomous devolved low-level decision-making and action. Soft robots face a similar challenge: Their high degrees of mechanical freedom would require a large number of communication channels to the central controller in order for it to control the body. A better solution is to adopt an octopus-inspired hierarchical system where sensing, decision-making, and action are undertaken within the distal limbs of the robot, as shown in Fig. 1A (ii). In such a robotic system, a central computer (higher-level controller) needs only consider high-level reasoning, and all other aspects of computation are devolved to the lower-level and distal parts of the body. Only minimum information is then transmitted through the body, such as action commands and perceptual feedback.

A key component in the octopus's hierarchical structure is the smart sucker. Each of the octopus's eight arms can be considered a series of segments, each consisting of a circumferential pair of

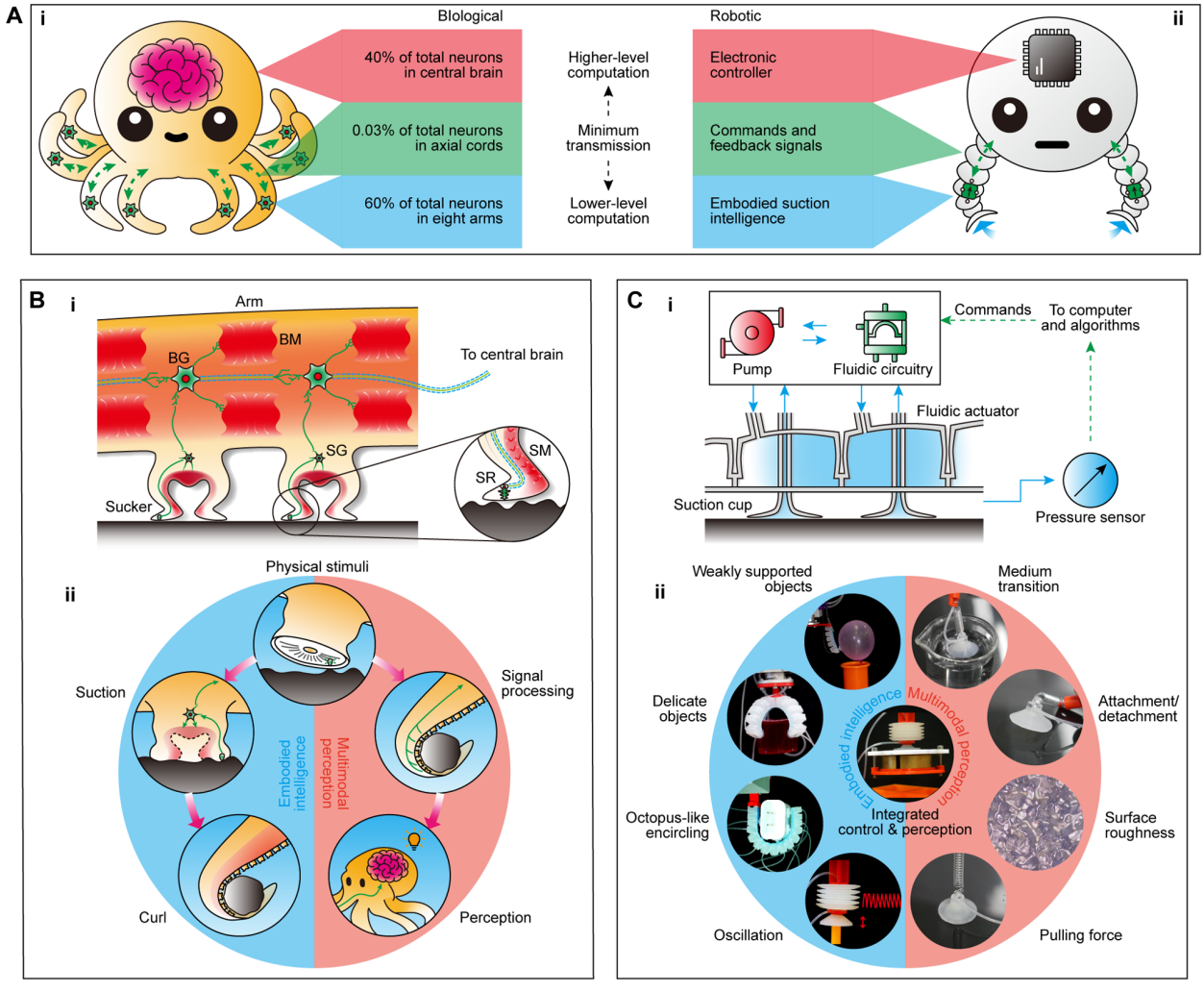

Fig. 1. Analog between the octopus and the proposed robotic suction intelligence. (**A**) Comparison between the hierarchical neural architecture of an octopus (i) and presented soft robotic suction intelligence (ii). (**B**) Biological structure (*5*, *10*) (i) and workflow (*3*, *5*, *7*) (ii) of octopus suction intelligence. The blue side of the diagram depicts the lower-level devolved in-arm embodied intelligence, and the orange side of the diagram depicts the sensing and higher-level decision-making. (**C**) Proposed robotic suction intelligence (i) and its octopus-like multimodal sensing and embodied intelligence (ii). The blue side of the diagram depicts the embodied intelligence for devolved action and control, and the orange side of the diagram depicts the higher-level multimodal sensing for environment monitoring.

sophisticated suckers. Sucker receptors (SRs) are distributed in the rim of the suckers and acquire environmental information (*10*). Nerve fibers connect sucker ganglions (SGs) and brachial ganglions (BGs) to SRs, sucker muscles (SMs), and brachial muscles (BMs) (*5*, *10*). The sucker neuromuscular circuit (SR, SG, and SM) predominantly controls suction, whereas the brachial circuit (BG and BM) largely controls arm articulation. Figure 1B (i) shows an axial slice through the arm with two suckers from neighboring segments. When a physical stimulus (for example, contact) occurs, processing occurs through two circuits. In one pathway, SGs generate local feedback signals to actuate colocated SMs; thereby the sucker automatically generates suction onto the contacting surface at the point of object detection. Control signals are transmitted to neighboring arm segments through the nerve cord, thereby generating a chain reaction of suction activation to gently encapsulate the object (*7*) [Fig. 1B (ii), embodied intelligence pathway]. Simultaneously in another pathway, sensory neural signals are generated by the SRs and filtered by the SGs and BGs. The preprocessed neural signals travel via the axial nerve cord and generate the higher-level perception of the touched object in the central brain (*5*) [Fig. 1B (ii), multimodal perception pathway]. The central brain makes higher-level decisions (*3*), whereas the lower-level computation is made within the local arm neural system. The versatility, efficiency, and adaptability of the octopus's devolved multilevel sensor-motor system inspired us to develop a robotic analogy. Such a system could reduce computation costs in the central processor (brain), increase manipulation speed through local sensing and actuation, increase robustness to unstructured environments, and facilitate more sophisticated and efficient body designs, which would otherwise incorporate excessive distal-to-proximal information and energy channels. An example of our presented octopus-inspired fluidic-driven (pneumatic or hydraulic) soft robotic system is shown in Fig. 1C (i). The system uses regular simple cups made from silicone to mimic octopus suckers. Soft fluidic actuators replicate the actions of BMs to articulate the robotic arm. Suction-triggered switches (STSs) mimic the BGs for embodied lower-level computation. Pressure sensors mimic SRs and acquire environmental information via suction flow. The computer and algorithms mimic the central brain and make higher-level decisions. Through this distributed and embedded system, soft robots can perform suction adhesion, perceive multimodal environmental information, and complete challenging tasks with a simple structure and low explicit (centralized) computational costs, as shown through the mimicked embodied intelligence and multimodal perception pathways of Fig. 1C (ii).

Low-level suction-based embodied intelligence

Octopuses locally exploit the rich sensory information from their sucker mechanoreceptors, enabling them to embody autonomous control within the arm. They can perform fast responses to external stimuli in local lower-level ganglia, without the need for higher-level computation in the central brain. In these autonomous behaviors, suckers act as "triggers" to convert environmental stimuli into neural signals for body control. Similarly, suction cups have a "triggering" effect on fluidic-driven soft robots—the suction seal can generate a sudden pressure drop and flow cutoff that can be used for physical computation, for example, in fluidic circuitries, without the need for electrical controllers. We demonstrate this concept via the following two designs.

First, we focus on a typical semiautonomous behavior of octopuses—autonomous suction—as shown in Fig. 2A (i). Once the octopus sucker contacts a surface, the SR-generated neural signals are processed by the local ganglia (*7*), which deactivate selected BMs from squeezing and simultaneously activate the SMs to capture the surface (*32*). In this way, octopuses can autonomously and gently grasp floating and delicate objects in the ocean. Our suction cups enable soft robots to mimic this behavior via a simple fluidic circuit, as shown in Fig. 2B and detailed in fig. S1. The outlet port of a diaphragm pump connects to one or more series-connected pneumatic actuators, and the inlet port connects to one or more series-connected suction cups. Once the suction cup contacted a smooth surface, a seal was established in a short time (<0.5 s), which simultaneously blocked the inflation of the pneumatic actuator. This structure allowed a single soft finger to gently grasp a weakly supported balloon without pushing it away, as shown in Fig. 2C and movie S1. A four-finger soft hand (fig. S1) involving multiple actuators and suction cups could gently and safely grasp delicate objects, such as a shell-less egg and even a brittle jelly [Fig. 2D (i) and (ii)]. Here, the robotic hand stopped squeezing once the fingertip suction cups contacted and established suction on the object, as shown in Fig. 2D (iii) and movie S2. In comparison, a regular soft robotic hand without fingertip suction cups applied uncontrollable squeezing force, which is harmful for delicate objects [Fig. 2D (iv)].

Another more complex semiautonomous behavior of octopuses is autonomous and simultaneous sucking and curling, as shown in Fig. 2A (ii). Once a sucker has established suction on the object, the neural signal emerging from the sucker activates a chain reaction in adjacent BGs via the axial nerve cord, stimulating neighboring BMs and causing the arm to encircle the object with a gentle shape adaptation. The autonomous sucking-curling occurs rapidly and smoothly because of the local low-level computation within the BGs. For a soft robot, the local computation can be achieved via STSs, which act as artificial "ganglia." An STS consists of three components as shown in Fig. 2E: top lid with inlet c and outlet d; bottom lid with inlet a and outlet b; and a silicone hemispherical snapping membrane, which separates the STS into upper and lower chambers. The pressure in the lower chamber (connecting a and b) controls the position of the membrane, which, in turn, controls the connection between ports c and d in the top chamber. As shown in Fig. 2E, when the bottom chamber is at ambient pressure (that is, a-b on), the membrane is in its rest (upper) state. The path c-d is off because of the strong sealing force applied by the membrane to the central hole (at port d) on the top lid. This seal ensures robust fluidic computation when port d applies a high vacuuming pressure. When the lower chamber is at negative pressure (that is, a-b off), the membrane snaps downward to open the path c-d. The working principle of the STS can be seen in movie S3. By using a snapping mechanism—analogous to thresholding within a neuron—STSs can execute fast and complex low-level preprogrammed computation when organized in parallel and series circuits, for example, the chain reaction as shown in Fig. 2F.

To demonstrate, we first designed a robotic hand that consists of four independent fingers (with fingertip suction cups), four diaphragm pumps, and three STSs. We used multiple pumps to generate independent fluidic flow. This eliminated channel interference and enabled better flexibility on spatial arrangements. Detailed structures are shown in fig. S2. These pumps were always on once powered and suitable for long-term use (see Supplementary

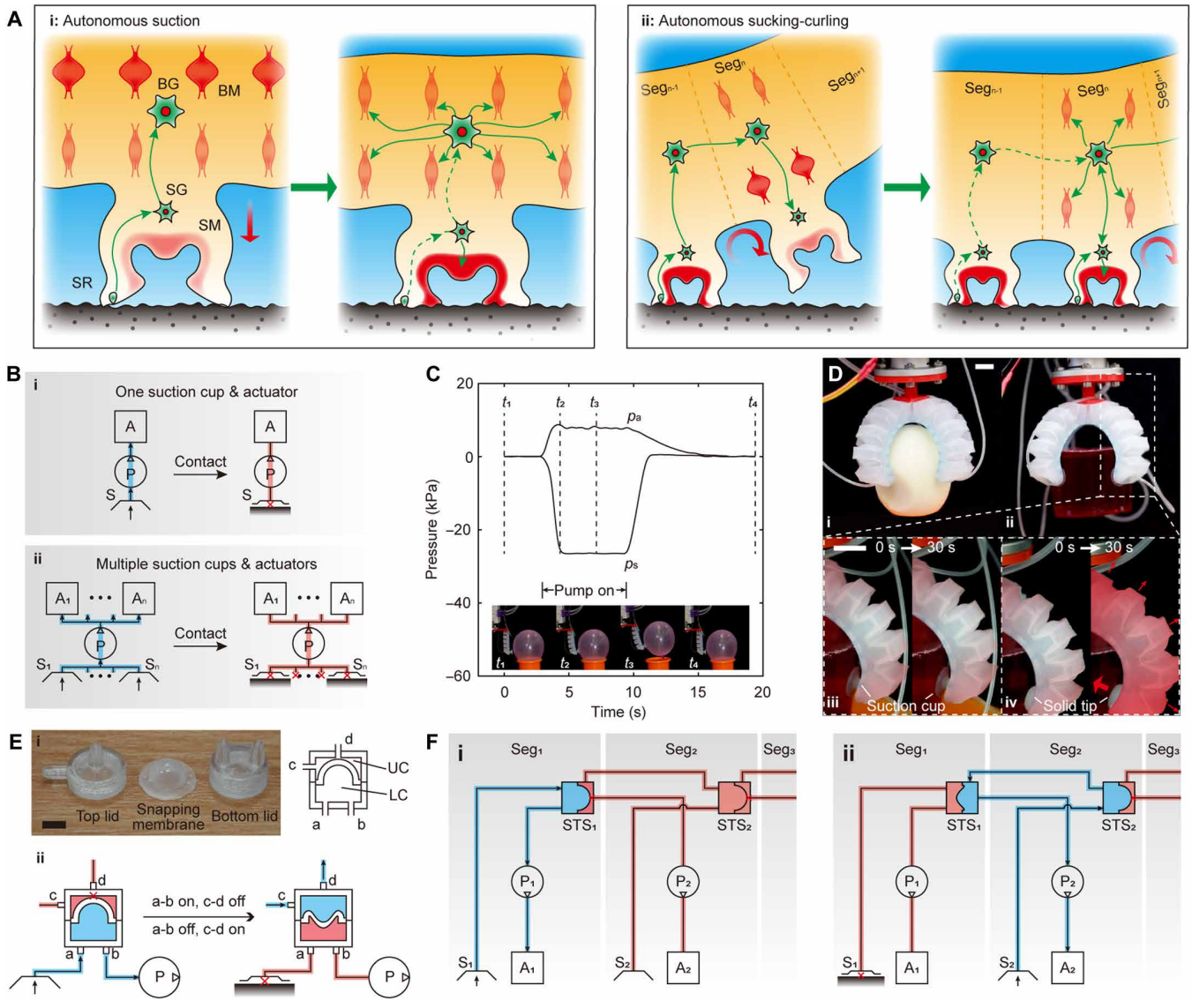

Fig. 2. Low-level suction-based embodied intelligence. (**A**) Octopus's autonomous suction (i) and autonomous sucking-curling (ii) behavior. (**B**) Fluidic circuit to achieve single-finger (i) and multifinger autonomous suction (ii). A, actuator; P, pump; S, suction cup. Blue and orange lines indicate open and blocked circuits, respectively. Cross marks indicate blocked points. (**C**) A single soft robotic finger gently grasps a weakly supported balloon. p_a, pressure in the actuator; p_s, pressure in the suction cup. (**D**) Soft robotic hand gently grasps a shell-less egg (i) and a soft jelly (ii), and the comparison between robotic hands with (iii) or without (iv) fingertip suction cups when grasping a jelly (shaded for clarity and indicating actuation and expansion). Scale bars, 10 mm. (**E**) Structure (i) and working principle (ii) of the STS. Scale bar, 5 mm. UC, upper chamber; LC, lower chamber. (**F**) Fluidic circuit using STSs to generate the intersegment chain reaction of actuation and suction. We only show the first two segments, the activation of the first (i), and the activation of the second (ii), because any number of segments can be added through the same configuration.

Methods). As shown in Fig. 3 (A and B), one finger first bent until its fingertip suction cup contacted the object. This contact triggered the first STS, which then triggered the next finger to begin to bend, with all fingers repeating this movement, until the object was gently grasped. In another configuration, as shown in Fig. 3C, an octopus arm–shaped robot with five independent segments was controlled by four STSs and actuated by five pumps. Once the pumps were powered on, the robot arm began to autonomously curl and suck onto the target object from the proximal end to the distal end, segment by segment. This movement generated an adaptive arm encirclement around unknown-shaped surfaces, enabling the squeezing force to be evenly and gently distributed on the object, successfully mimicking the octopus's semiautonomous sucking and curling behavior. Furthermore, the pumps, battery, and STSs can be integrated into a compact, intelligent robotic hand without requiring an electric controller, as illustrated in Fig. 3 (D and E). The STS design is scalable, as demonstrated in Fig. 3D (iii), where all dimensions were reduced to half, resulting in a volume that is just one-eighth (that is, an 87.5% reduction) of the original. The adaptive grasping can be seen in movie S4.

Suction-based multimodal perception

For both octopus suckers and artificial suction cups, perception is based on decoding measurable physical quantities. Octopus SRs can

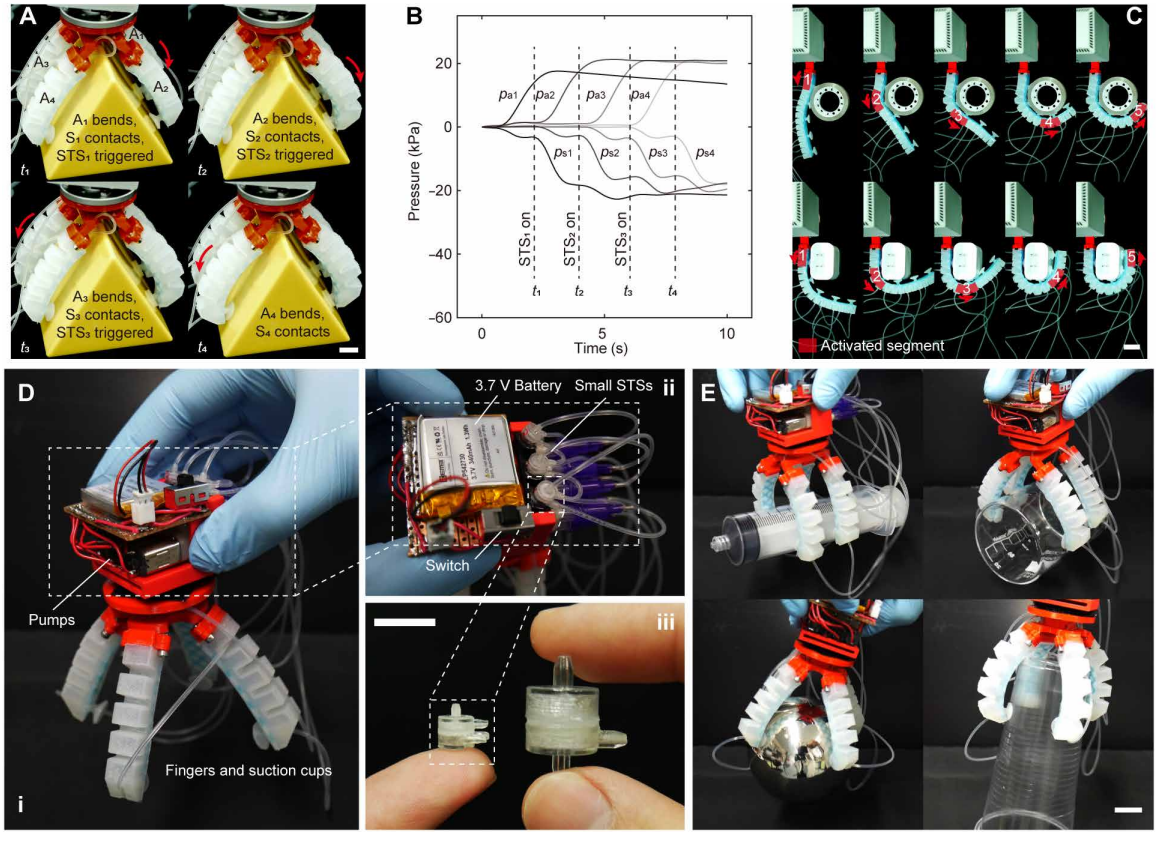

Fig. 3. STS-enhanced embodied intelligence of soft robots. (**A**) Adaptive grasping of the four-finger robotic hand. t_1 to t_4, where t is time, correspond to the annotation in (B). Scale bar, 10 mm. (**B**) Measured pressure of the four-finger robotic hand, grasping the object by autonomously recruiting more fingers, one by one. (**C**) Autonomous and adaptive curling and sucking on different objects of the five-segment robotic arm. Scale bar, 20 mm. (**D**) Integration of a suction-embodied intelligent robotic hand. (i) Overview of the whole structure, (ii) top view of the integration, and (iii) comparison between a smaller STS and a larger STS. Scale bar, 10 mm. (**E**) Using the integrated intelligent robotic hand to gently pick up four different-shaped objects. Scale bar, 20 mm.

be considered stretch sensors (*10*) that convert cell deformation into neural signals for transmission to and decoding by the central brain. Accurately replicating the octopus's deformation-induced mechanoreceptors would require complex in-sucker transducers. Alternatively, fluid-based sensing (*15*–*19*) (measuring the suction fluidic pressure by pressure sensors) can directly convert pressure in and around the suction cup into electric signals that reflect the physical interaction between the suction cup and environment. It provides a much simpler way for robots to perceive multiple environmental conditions.

As shown in Fig. 4A, when a suction cup (with a hole in the center) is evacuated by a pump, the measured pressure p_m via a pressure sensor is defined by $p_m = p_s - p_e$, where p_s and p_e are the pressure at the suction cup and environment, respectively. Typical application scenarios of a suction cup can be classified into two cases, as shown in Fig. 4B. For case 1 (noncontacting), the suction cup is continuously sucking in environmental medium through the central hole, and therefore p_m is dominated by the pressure drop in the thin tube from the sensor (where p_s is measured) to the suction cup's opening hole (where p_e is measured). In this case, the measured pressure is related to the environmental medium viscosity μ, that is, $p_{m,case\ 1} = f_1(\mu)$. For case 2 (contacting a surface and being pulled by a force F_{pull}), the suction cup is sucking in environmental medium through the thin aperture between the disc and substrate, inside the ring-shaped sealing region (the gray part in the bottom view of fig. S3). In this case, the measured pressure is related to three variables: the environmental medium viscosity μ, the contacting surface roughness R, and the pulling force F_{pull}, that is, $p_{m,case\ 2} = f_2(\mu, R, F_{pull})$. The theoretical derivation is provided in the Supplementary Methods (*33*, *34*). In summary, the environmental medium (reflected by fluid viscosity), the contacting surface roughness, and the pulling force, as well as the occurrence of contact (the state transition between case 1 and case 2), can be perceived by analyzing the measured p_m signal.

To demonstrate, we collected p_m signals with different combinations of environmental medium (air or water), surface roughness (sandpaper with 320, 400, 600, 800, or 1000 grit), and pulling force. The user manually moved a suction cup (as shown in Fig. 4C) down and up to suck onto, and break away from, the rough sandpaper. During this period, p_m and F_{pull} signals were collected. Two examples of the collected signals are shown in Fig. 4D [(i) and (ii) illustrate the wet and dry cases, respectively]. When the suction cup was moved from air to water [P_2 to P_3 in Fig. 4D (i)], we observed a large and rapid decrease in p_m. When the suction cup contacted sandpaper [P_4 to P_5 in Fig. 4D (i) and (ii)], we observed a step decrease in p_m, the shape of which was affected by both the surface roughness and environmental medium (air or water). When the suction cup was pulled in the dry case [P_6 to P_7 in Fig. 4D (ii)], we observed that

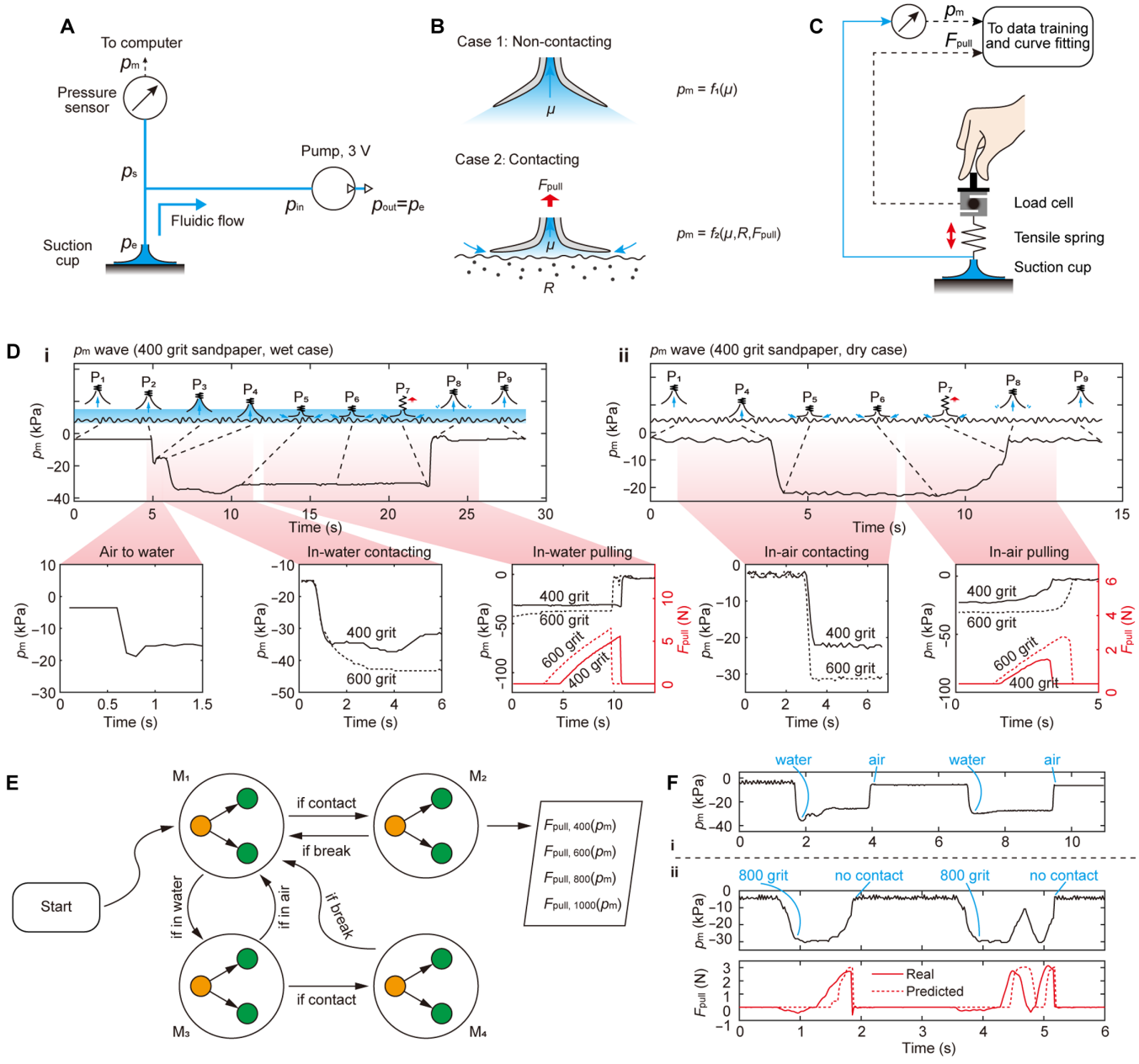

Fig. 4. Suction-based multimodal sensing. (**A**) Prototype of suction-based multimodal perception. (**B**) Diagrams of the two cases of suction cup application scenarios. (**C**) Experimental setup for collecting data for training and modeling. The pump is not shown. (**D**) Two examples of p_m waves when the suction cup is tested in a wet case (i) and dry case (ii). Points P_1 through P_9 denote the key moments of the following states: start, before transition to water, after transition to water, before contact, after contact, before pulling, before breaking, after breaking, and end. P_2 and P_3 only work for the wet case. Inset graphs show the zoomed-in details of different periods. Dashed lines were measured from substrates with 600-grit roughness for comparison [not drawn in (i) and (ii)]. Time axes for all of the inset graphs begin from 0 s. (**E**) Workflow of the four classifiers. (**F**) Using the presented multimodal perception algorithm to detect unknown environmental conditions. (i) Environmental medium transition test. (ii) In-air contacting test. Blue text indicates detected information.

p_m changed with the pulling force until the suction cup broke away from the sandpaper. When the suction cup was pulled in the wet case [P_6 to P_7 in Fig. 4D (i)], we did not observe a distinct relation between F_{pull} and p_m, indicating that the in-water pulling force prediction was not applicable. p_m exhibited different signals under different environmental conditions, and we next explored how this time-domain information could be used to facilitate suction-based multimodal perception.

The designs of the perception method are detailed in the Supplementary Methods and figs. S4 and S5. Here, we highlight only the key principles. Changes in the environmental medium, the occurrence of contact, and the surface roughness were determined through classification models, M_1 to M_4, as shown in Fig. 4E. Some occurrences of the events are mutually exclusive; for example, the in-water contact can only occur when the suction cup has been moved into water and cannot occur when the suction cup is in air.

Therefore, using four simple classifiers, M_1 to M_4, could improve the classification accuracy and reduce system complexity. Here, we used small decision trees, but other simple classifiers such as neural networks could be used. M_1 and M_3 were used to classify the events occurring in air and in water, respectively, whereas M_2 and M_4 were used to classify the surface roughness in air and in water, respectively. M_1 to M_3 achieved a mean accuracy of >95% (fig. S4, F to H), whereas M_4 (classifying surface roughness underwater) had a lower mean accuracy of ~71% (fig. S4I). The change in the pulling force could be modeled through curve fitting. Power models (applicable for the dry cases) were used to fit the measured $F_{pull} - p_m$ curves on 400-, 600-, 800-, and 1000-grit surfaces (fig. S5), whereas the case for 320 grit was inapplicable because the seal was too weak. By organizing the classifiers and fitted functions, the workflow as shown in Fig. 4E could be used to predict previously unidentified signals. As shown in Fig. 4F and movie S5, the algorithm successfully perceived the transition between air and water, perceived the contact, and determined the surface roughness. Trends in the pulling force were predicted, although the predicted value had a mean error of ~27%, as measured from the three force peaks shown in Fig. 4F.

Hierarchical soft robotic system enhanced by suction intelligence

The suction-based embodied intelligence and multimodal perception, respectively, use the energy (pressure change) and information (pressure signal) of the suction flow, making it possible to integrate the two functionalities into one system without affecting each other. Here, we demonstrated this concept using an octopus-like hierarchical soft robotic system. Throughout, the fundamental suction adhesion functionality was unaltered. Such a system integrates suction adhesion, embodied intelligence, and multimodal perception. It only requires a higher-level controller to generate the general command and undertake perceptual processing, whereas the lower-level embodied intelligence simultaneously carries out the commanded or reflexive behavior and collects environmental information.

We demonstrated this hierarchical intelligence in a simple system as shown in Fig. 5A (i), which consisted of a computer (the higher-level controller), an STS (the lower-level controller), two pumps, and a soft gripper. The detailed structure is shown in fig. S6. As shown in Fig. 5A (ii), when the computer sent the command to power the two pumps, the STS blocked the evacuating flow from pump 1, and therefore the inflating flow from pump 2 made the actuator extend. Because the STS only stopped evacuating flow from pump 1 and did not completely prevent the inflating flow from pump 2, the actuator extended until it reached a balanced position. Once the suction cup contacted and captured the object (which blocked the inflating flow from pump 2), the STS switched to open the pathway from pump 1 and made the actuator retract. Pressure signals during this process were sent to the computer for sensing (using the same method as before; see Supplementary Methods); therefore, the computer could perceive the wetness, mass, and surface roughness of the gripped object with relatively high accuracy (mean > 89%), as shown in Fig. 5B and movie S6.

The hierarchical architecture allowed other interesting behaviors. When the target contacting area was small (here, we used a round-head pin with a diameter of 8 mm as shown in Fig. 5C and movie S7), the STS could be triggered, but the suction cup could not generate a strong enough adhesion to pick the object up. This caused the STS to continuously switch between the open and closed states, making the actuator switch between extending and retracting. As a result, the suction cup oscillated rapidly around the contacting position. Driven by 3-V pumping, the oscillating displacement (d_o) of this gripper was measured at a frequency of 3.4 Hz and amplitude of 0.2 mm. The oscillation was also self-positioning: When the upper end of the actuator was moved by a robotic arm, the actuator automatically adjusted its length to make the oscillation always occur at the contacting site. All of the movement was coordinated by the lower-level controller STS, without the control of the higher-level controller. When the p_m signal was sent to and processed by the computer via a high-pass filter (labeled $p_{highpass}$), the movement of the actuator upper end could be detected. This information, processed by the higher-level controller, enabled the robot to understand its surrounding environment and make suitable action decisions. This autonomous retraction also achieved gentle responsive interaction with the human finger, as shown in Fig. 5D and movie S8. Gently contacting the suction hole caused the actuator to retract. When the fingertip was removed, the STS switched the actuator to reextend until it reached its equilibrium position.

DISCUSSION

The hierarchical neural architecture and embodied computation and control of the octopus are attractive for replication in soft robots. Fluidic-based embodied control (using fluidic energy) (*20*–*27*, *35*–*38*) and fluidic-based sensing (using fluidic information) (*15*–*19*) have been separately demonstrated in previous research. However, limited research has been done to leverage the two properties in one system, let alone further combine them with suction adhesion functionality. Fluidic flow is both energy-rich and information-rich, and through our work, we demonstrate its capability to combine the octopus-like low-level embodied intelligence and higher-level perception in a highly integrated form. We exploit the suction seal that forms at the moment of contact, which provides a rapid binary pressure signal to trigger robust fluidic computation. Implicit sensing by integrating simple suction cups enables the robot to "sense" environmental changes and act accordingly without explicitly outputting data. Thus, we can achieve octopus-like lower-level interactive embodied intelligence, including delicate multifinger gripping and adaptively encircling unknown objects. In addition, explicit sensing incorporating a pressure sensor can provide detailed signals for higher-level perception under multiple environmental conditions, including contact, environmental medium, surface roughness, and pulling force. The small suction region enables the suction-based perception to have higher sensitivity than previous fluid-based perception methods (*39*–*41*). Last, we demonstrated that suction-based adhesion, embodied intelligence, and multimodal perception can be integrated into a simple but comprehensive hierarchical system.

The presented soft autonomy mimics the general architecture of the octopus neuromuscular system, where the central brain or computer is reserved for higher-level perception and decision-making, whereas embedded STSs (artificial ganglia) handle lower-level signal processing and control. The suction cups, pressure sensors, STSs, and pumps function analogously to the octopus's suckers, SRs, ganglia, and muscles. The primary difference lies in the realization of control and actuation in the low-level autonomy. In octopus biology, control (by neurons) and actuation (by muscles) are distinct

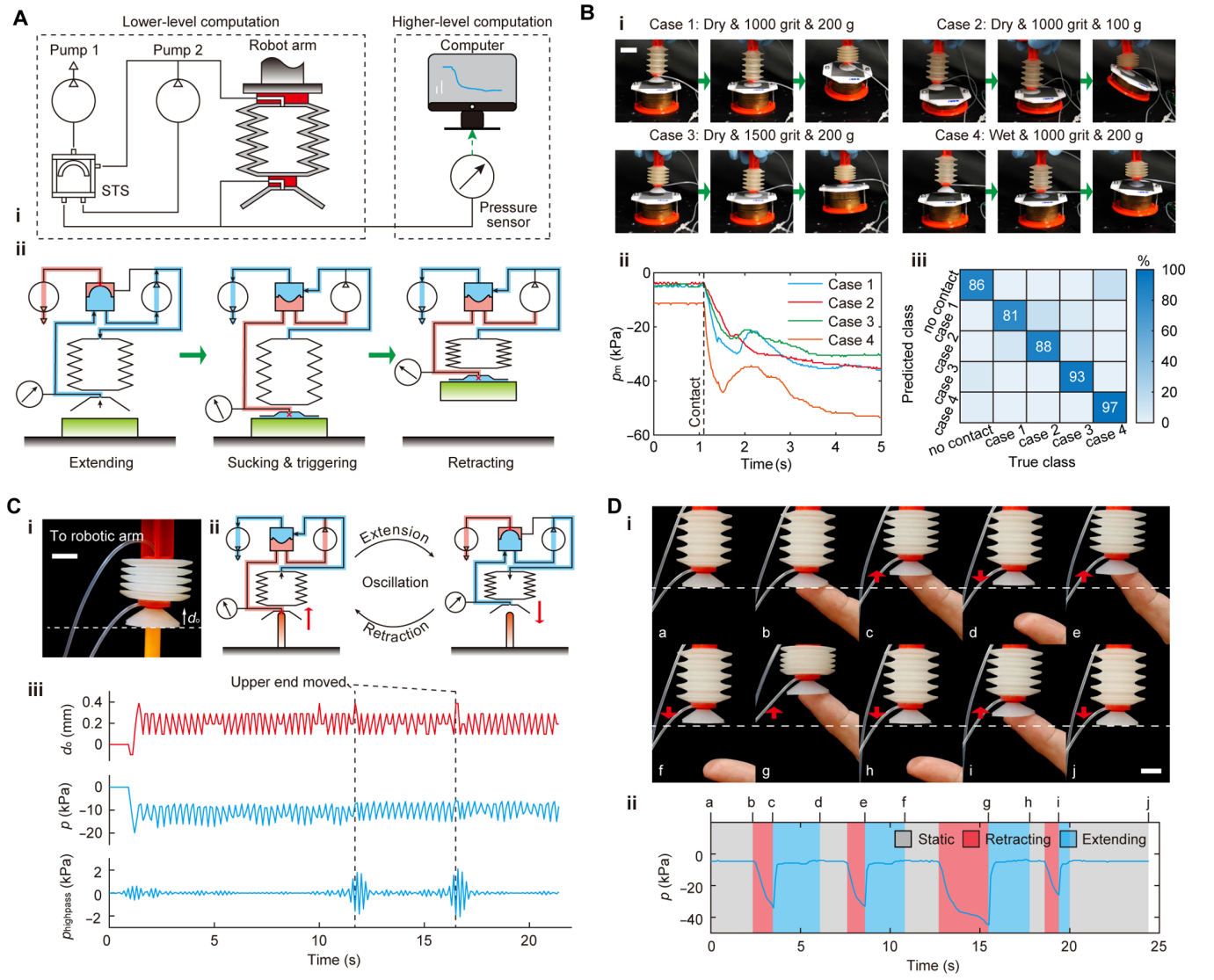

Fig. 5. Integrated suction-based multimodal perception and embodied intelligence. (**A**) Prototype of the simple soft robotic gripper. (**B**) Integrating the embodied intelligence, multimodal sensing, and suction adhesion in one soft gripper. (i) Photos of the gripper automatically executing the extend-suck-retract behavior. The maximum inflation situation can be seen in cases 1, 2, and 4. Scale bar, 20 mm. (ii) Example raw signals of the four cases. (iii) The trained classification model. (**C**) Application of the simple soft robot as a self-positioning oscillator with movement detection. (i) The setup. Scale bar, 10 mm. (ii) The working principle of the oscillation. (iii) The recorded signals during the oscillation. (**D**) Gentle responsive interaction of the gripper with the human finger. (i) The snapshots. Scale bar, 10 mm. (ii) The recorded suction pressure.

systems coordinated by neural signals. Conversely, our strategy integrates fluidic flow to embody both control (via STSs) and actuation (through soft actuators) circuits. This approach is highly suitable for soft robots, enabling them to perform a wide range of practical tasks using simple, non–electronic-controller architectures.

In contrast with previous studies on fluidic-based embodied intelligence (see table S2), the presented hierarchical sucker intelligence shows advantages in terms of system complexity and multifunctionality. From capturing weakly supported and delicate objects (Fig. 2) to responsively and sequentially actuating multisegment robots (Fig. 3), the suction intelligence demonstrated its low-level autonomy well. Integrating with suction-based multimodal perception, the intelligent suction gripper (Fig. 5) provides a low-cost solution for industrial robots to complete autonomous gripping tasks while simultaneously identifying object features. The flexible programmability by simply reconfiguring STSs has great potential for developing advanced smart fluidic actuators and, together with the presented hierarchical intelligence system, can enable a next generation of soft robots with advanced perception, devolved control, and autonomous behaviors.

We achieved multimodal perception on contact, environmental medium, surface roughness, and pulling force via a simple suction pressure signal. The in-air perception exhibited faster response times (0.44 s in air and 3.06 s in water) and higher classification accuracy than in water, as detailed in the Supplementary Methods and figs. S4 and S5. This is attributed to the notably lower viscosity of air

compared with water, ~55 times lower, which allowed the system to reach equilibrium more quickly. The incompressibility of water also creates pressures that exceed the diaphragm pump's capacity, leading to challenges in predicting pulling forces underwater, whereas capturing the in-air pulling force and its trends is accessible (Fig. 4F). However, limited by the fidelity of information provided by the one-dimensional suction signal, the perception is not as accurate as purpose-designed sensors. The primary focus of our study was to explore the underlying physics of suction-based sensing, with sensing being just one component of the broader suction intelligence framework. Its simplicity and integration with embodied intelligence and suction adhesion will provide different perspectives in soft robots.

The proposed approach can be further improved through the following aspects in the future. The tubes were intentionally left relatively long for early-stage demonstrations. Future applications should consider embedding the tubes within chambers (*42*). The size of the STS can be further scaled down, leveraging its snapping structure to achieve a more compact design. In addition, although suction cups have some adaptability to the surface morphology (figs. S7 to S10), suction failure was observed under several difficult conditions (fig. S11). Future work should explore integrating higher-level active control (*28*, *42*–*50*) with the current lower-level suction intelligence to improve adaptability (table S3). Furthermore, the lower-level autonomy could be expanded from the current sequential triggering mechanism to a parallel triggering approach (such as shown in fig. S12), enabling the robot to achieve greater grasping flexibility. Perception using multiple suckers is also a promising avenue for future research. However, the classifier seems transferable only between highly identical suckers (fig. S13); otherwise, individually trained models will be required for each sucker.

In this work, we demonstrated that suction-based soft robotic systems can integrate embodied computation, multimodal perception, and suction adhesion within a unified architecture. This approach enables autonomous interaction with uncertain and delicate environments without relying on complex centralized computation or electronic control. Our findings highlight the potential of bioinspired hierarchical control to advance the adaptability and robustness of future soft robotic systems, offering different insights into the design of multifunctional intelligent machines.

MATERIALS AND METHODS

Design, materials, and electronics of the soft robotic system

Detailed setups and designs of the soft robotic system are presented in the Supplementary Methods. Suction cups, fluidic actuators, and snapping membranes in larger STSs were made by casting silicone (Dragon Skin 10 NV, Smooth-on). Snapping membranes in smaller STSs were made by casting a softer silicone (Ecoflex 00-50, Smooth-on). The shells of the STSs were 3D printed from VeroClear (J826, Stratasys). The actuator used in Fig. 5 was 3D printed from Agilus with a Shore hardness of 60A (J826, Stratasys). Other rigid parts were 3D printed (i3 Mega S, Anycubic) with polylactic acid (PLA). Tubes (Hilltop) had an inner diameter of 0.4 mm and a wall thickness of 0.3 mm. Diaphragm pumps (SC0801XPW, SKOOCOM) were powered with 3 V for all experiments. Two types of pressure sensors were used. Sensor SSCDRRV015PDAA5 (Honeywell) was capable of measuring both air and clean liquids and was used in all experiments involving water, such as in Fig. 4D (i). Sensor XGZ-P6847A100KPG (Yijiajie) could only be used in dry air and was used only in dry experiments, such as in Fig. 3B. An Arduino Nano was used to receive data from pressure sensors.

Smoothing suction cups and snapping membranes

The bottom surface of suction cups and the convex side of the snapping membrane must be smooth because they are used to establish a seal with the substrate. Molds were 3D printed (Ultimaker 3) from acrylonitrile butadiene styrene (ABS) with the highest resolution (layer height of 0.06 mm) and then sprayed with acetone several times to smooth the surface until no layer textures were visible. The suction cups and snapping membranes were then cast in these smoothed molds with silicone.

Data collection

For the multimodal perception experiments in Fig. 4C, the data for machine learning were collected as follows. Rough surfaces were made by attaching 320-, 400-, 600-, 800-, or 1000-grit sandpaper (HU-XI-50, Cymax) to acrylic plates. For the water case, the sandpaper was attached to the bottom of a water tank, in which the depth of the water was ~1 cm. The following experimental processes were repeated 100 times for each combination of rough surface and air or water case. A small 3-V diaphragm pump was used to generate suction flow via a suction cup with a diameter of 20 mm. The user manually carried a load cell (with a range of 1 kg, Uxcell) for measuring the pulling force, below which a tensile spring connected to a suction cup. The suction cup was moved to transition between air and water (in a tank); it was then moved down until it just achieved suction on the rough surface, and then it was pulled until breaking away from the substrate. Pressure signals and pulling force during the experiment were collected with a 45.8-Hz sampling frequency. For the gripping experiments in Fig. 5B, the gripper was carried by hand to introduce randomness. Different inflation situations, especially the highly inflated conditions (when the actuator was inflated to reach the balanced position), were intentionally explored. An object was prepared with one or two 100-g masses on it, and 1000- or 1500-grit sandpaper was attached to the top of the mass. The sandpaper was manually wetted or dried to create different conditions. Each experiment was repeated 100 times. Collected raw data were then prepared to train the classification models as detailed in the Supplementary Methods.

Statistical analysis

For the classification tasks, raw data were manually labeled and partitioned into training (90%) and testing datasets (10%) to avoid overfitting. Pressure signals were segmented using sliding windows of different lengths depending on the environmental condition, according to table S1. Feature extraction and data preparation were then performed accordingly. Classification models were trained using the built-in fine–decision tree function in MATLAB. For suction-based force estimation, pressure-force signal pairs were extracted during the pulling period and fitted using power functions. The resulting models were used for classification and regression tasks within the perception framework. For the hierarchical intelligent gripping experiments, the same data processing pipeline was applied with adjusted window lengths. SDs of all experiments involving repeated measurements are represented as error bars in the corresponding figures, with sample sizes (N) indicated in the figure

captions. Full details of the data processing, slicing, model training, and fitting procedures are provided in the Supplementary Methods.

Supplementary Materials

The PDF file includes:
Supplementary Methods
Figs. S1 to S17
Tables S1 to S3
Legends for movies S1 to S8

Other Supplementary Material for this manuscript includes the following:
Movies S1 to S8

REFERENCES AND NOTES

1. G. Sumbre, G. Fiorito, T. Flash, B. Hochner, Motor control of flexible octopus arms. *Nature* **433**, 595–596 (2005).
2. S. van Veggel, M. Wiertlewski, E. L. Doubrovski, A. Kooijman, E. Shahabi, B. Mazzolai, R. B. N. Scharff, Classification and evaluation of octopus-inspired suction cups for soft continuum robots. *Adv. Sci.* **11**, 2400806 (2024).
3. B. Hochner, An embodied view of octopus neurobiology. *Curr. Biol.* **22**, R887–R892 (2012).
4. T. Gutnick, L. Zullo, B. Hochner, M. J. Kuba, Use of peripheral sensory information for central nervous control of arm movement by *Octopus vulgari*. *Curr. Biol.* **30**, 4322–4327.e3 (2020).
5. G. Sumbre, Y. Gutfreund, G. Fiorito, T. Flash, B. Hochner, Control of octopus arm extension by a peripheral motor program. *Science* **293**, 1845–1848 (2001).
6. L. van Giesen, P. B. Kilian, C. A. H. Allard, N. W. Bellono, Molecular basis of chemotactile sensation in octopus. *Cell* **183**, 594–604.e14 (2020).
7. A.-S. Darmaillacq, L. Dickel, J. Mather, *Cephalopod Cognition* (Cambridge Univ. Press, 2014).
8. A. Kuuspalu, S. Cody, M. E. Hale, Multiple nerve cords connect the arms of octopuses, providing alternative paths for inter-arm signaling. *Curr. Biol.* **32**, 5415–5421.e3 (2022).
9. P. Graziadei, Electron microscopy of some primary receptors in the sucker of *Octopus vulgaris*. *Cell Tissue Res.* **64**, 510–522 (1964).
10. P. P. Graziadei, H. T. Gagne, Sensory innervation in the rim of the octopus sucker. *J. Morphol.* **150**, 639–679 (1976).
11. Z. Xie, F. Yuan, J. Liu, L. Tian, B. Chen, Z. Fu, S. Mao, T. Jin, Y. Wang, X. He, G. Wang, Y. Mo, X. Ding, Y. Zhang, C. Laschi, L. Wen, Octopus-inspired sensorized soft arm for environmental interaction. *Sci. Robot.* **8**, eadh7852 (2023).
12. E. Shahabi, F. Visentin, A. Mondini, B. Mazzolai, Octopus-inspired suction cups with embedded strain sensors for object recognition. *Adv. Intell. Syst.* **5**, 2200201 (2023).
13. H. J. Lee, S. Baik, G. W. Hwang, J. H. Song, D. W. Kim, B.-y. Park, H. Min, J. K. Kim, J.-s. Koh, T.-H. Yang, An electronically perceptive bioinspired soft wet-adhesion actuator with carbon nanotube-based strain sensors. *ACS Nano* **15**, 14137–14148 (2021).
14. J. C. Tuthill, E. Azim, Proprioception. *Curr. Biol.* **28**, R194–R203 (2018).
15. H. S. Stuart, M. Bagheri, S. Wang, H. Barnard, A. L. Sheng, M. Jenkins, M. R. Cutkosky, "Suction helps in a pinch: Improving underwater manipulation with gentle suction flow," in *2015 IEEE/RSJ International Conference on Intelligent Robots and Systems (IROS)* (IEEE, 2015), pp. 2279–2284.
16. P. Nadeau, M. Abbott, D. Melville, H. S. Stuart, "Tactile sensing based on fingertip suction flow for submerged dexterous manipulation," in *2020 IEEE International Conference on Robotics and Automation (ICRA)* (IEEE, 2020), pp. 3701–3707.
17. H. S. Stuart, S. Wang, M. R. Cutkosky, Tunable contact conditions and grasp hydrodynamics using gentle fingertip suction. *IEEE Trans. Robot.* **35**, 295–306 (2018).
18. T. M. Huh, K. Sanders, M. Danielczuk, M. Li, Y. Chen, K. Goldberg, H. S. Stuart, "A multi-chamber smart suction cup for adaptive gripping and haptic exploration," in *2021 IEEE/RSJ International Conference on Intelligent Robots and Systems (IROS)* (IEEE, 2021), pp. 1786–1793.
19. J. Lee, S. D. Lee, T. M. Huh, H. S. Stuart, Haptic search with the smart suction cup on adversarial objects. *IEEE Trans. Robot.* **40**, 226–239 (2023).
20. D. Drotman, S. Jadhav, D. Sharp, C. Chan, M. T. Tolley, Electronics-free pneumatic circuits for controlling soft-legged robots. *Sci. Robot.* **6**, eaay2627 (2021).
21. J. D. Hubbard, R. Acevedo, K. M. Edwards, A. T. Alsharhan, Z. Wen, J. Landry, K. Wang, S. Schaffer, R. D. Sochol, Fully 3D-printed soft robots with integrated fluidic circuitry. *Sci. Adv.* **7**, eabe5257 (2021).
22. W.-K. Lee, D. J. Preston, M. P. Nemitz, A. Nagarkar, A. K. MacKeith, B. Gorissen, N. Vasios, V. Sanchez, K. Bertoldi, L. Mahadevan, G. M. Whitesides, A buckling-sheet ring oscillator for electronics-free, multimodal locomotion. *Sci. Robot.* **7**, eabg5812 (2022).
23. B. Mosadegh, C.-H. Kuo, Y.-C. Tung, Y.-s. Torisawa, T. Bersano-Begey, H. Tavana, S. Takayama, Integrated elastomeric components for autonomous regulation of sequential and oscillatory flow switching in microfluidic devices. *Nat. Phys.* **6**, 433–437 (2010).
24. D. J. Preston, P. Rothemund, H. J. Jiang, M. P. Nemitz, J. Rawson, Z. Suo, G. M. Whitesides, Digital logic for soft devices. *Proc. Natl. Acad. Sci. U.S.A.* **116**, 7750–7759 (2019).
25. P. Rothemund, A. Ainla, L. Belding, D. J. Preston, S. Kurihara, Z. Suo, G. M. Whitesides, A soft, bistable valve for autonomous control of soft actuators. *Sci. Robot.* **3**, eaar7986 (2018).
26. M. Wehner, R. L. Truby, D. J. Fitzgerald, B. Mosadegh, G. M. Whitesides, J. A. Lewis, R. J. Wood, An integrated design and fabrication strategy for entirely soft, autonomous robots. *Nature* **536**, 451–455 (2016).
27. Y. Zhai, A. De Boer, J. Yan, B. Shih, M. Faber, J. Speros, R. Gupta, M. T. Tolley, Desktop fabrication of monolithic soft robotic devices with embedded fluidic control circuits. *Sci. Robot.* **8**, eadg3792 (2023).
28. F. Liu, F. Sun, B. Fang, X. Li, S. Sun, H. Liu, Hybrid robotic grasping with a soft multimodal gripper and a deep multistage learning scheme. *IEEE Trans. Robot.* **39**, 2379–2399 (2023).
29. S. T. Frey, A. B. M. T. Haque, R. Tutika, E. V. Krotz, C. Lee, C. B. Haverkamp, E. J. Markvicka, M. D. Bartlett, Octopus-inspired adhesive skins for intelligent and rapidly switchable underwater adhesion. *Sci. Adv.* **8**, eabq1905 (2022).
30. S. Baik, D. W. Kim, Y. Park, T.-J. Lee, S. Ho Bhang, C. Pang, A wet-tolerant adhesive patch inspired by protuberances in suction cups of octopi. *Nature* **546**, 396–400 (2017).
31. J. Z. Young, *Anatomy of the Nervous System of Octopus vulgaris* (Clarendon Press, 1971).
32. D. M. Sivitilli, T. Strong, W. Weertman, J. Ullmann, J. R. Smith, D. H. Gire, Mechanisms of octopus arm search behavior without visual feedback. *Bioinspir. Biomim.* **18**, 066017 (2023).
33. A. Tiwari, B. N. J. Persson, Physics of suction cups. *Soft Matter* **15**, 9482–9499 (2019).
34. C. Yang, B. N. J. Persson, Contact mechanics: Contact area and interfacial separation from small contact to full contact. *J. Phys. Condens. Matter* **20**, 215214 (2008).
35. Z. Jiao, Z. Hu, Y. Shi, K. Xu, F. Lin, P. Zhu, W. Tang, Y. Zhong, H. Yang, J. Zou, Reprogrammable, intelligent soft origami LEGO coupling actuation, computation, and sensing. *Innovation* **5**, 100549 (2024).
36. M. Pontin, D. D. Damian, Multimodal soft valve enables physical responsiveness for preemptive resilience of soft robots. *Sci. Robot.* **9**, eadk9978 (2024).
37. A. A. Stanley, E. S. Roby, S. J. Keller, High-speed fluidic processing circuits for dynamic control of haptic and robotic systems. *Sci. Adv.* **10**, eadl3014 (2024).
38. L. C. van Laake, J. de Vries, S. M. Kani, J. T. B. Overvelde, A fluidic relaxation oscillator for reprogrammable sequential actuation in soft robots. *Matter* **5**, 2898–2917 (2022).
39. C. Tawk, E. Sariyildiz, G. Alici, Force control of a 3D printed soft gripper with built-in pneumatic touch sensing chambers. *Soft Robot.* **9**, 970–980 (2022).
40. C. Tawk, G. Alici, A review of 3D-printable soft pneumatic actuators and sensors: Research challenges and opportunities. *Adv. Intell. Syst.* **3**, 2000223 (2021).
41. S. Zou, S. Picella, J. de Vries, V. G. Kortman, A. Sakes, J. T. B. Overvelde, A retrofit sensing strategy for soft fluidic robots. *Nat. Commun.* **15**, 539 (2024).
42. H. Jiang, Z. Wang, Y. Jin, X. Chen, P. Li, Y. Gan, S. Lin, X. Chen, Hierarchical control of soft manipulators towards unstructured interactions. *Int. J. Robot. Res.* **40**, 411–434 (2021).
43. P. Wang, Z. Xie, W. Xin, Z. Tang, X. Yang, M. Mohanakrishnan, S. Guo, C. Laschi, Sensing expectation enables simultaneous proprioception and contact detection in an intelligent soft continuum robot. *Nat. Commun.* **15**, 9978 (2024).
44. Y. Cui, X. An, Z. Lin, Z. Guo, X.-J. Liu, H. Zhao, Design and implementation of an underactuated gripper with enhanced shape adaptability and lateral stiffness through semi-active multi-degree-of-freedom endoskeletons. *Int. J. Robot. Res.* **43**, 873–896 (2024).
45. Y. Cui, X.-J. Liu, X. Dong, J. Zhou, H. Zhao, Enhancing the universality of a pneumatic gripper via continuously adjustable initial grasp postures. *IEEE Trans. Robot.* **37**, 1604–1618 (2021).
46. X. Guo, W. Tang, K. Qin, Y. Zhong, H. Xu, Y. Qu, Z. Li, Q. Sheng, Y. Gao, H. Yang, J. Zou, Powerful UAV manipulation via bioinspired self-adaptive soft self-contained gripper. *Sci. Adv.* **10**, eadn6642 (2024).
47. J. M. Romano, K. Hsiao, G. Niemeyer, S. Chitta, K. J. Kuchenbecker, Human-inspired robotic grasp control with tactile sensing. *IEEE Trans. Robot.* **27**, 1067–1079 (2011).
48. S. Suresh, H. Qi, T. Wu, T. Fan, L. Pineda, M. Lambeta, J. Malik, M. Kalakrishnan, R. Calandra, M. Kaess, J. Ortiz, M. Mukadam, NeuralFeels with neural fields: Visuotactile perception for in-hand manipulation. *Sci. Robot.* **9**, eadl0628 (2024).
49. C. B. Teeple, T. N. Koutros, M. A. Graule, R. J. Wood, Multi-segment soft robotic fingers enable robust precision grasping. *Int. J. Robot. Res.* **39**, 1647–1667 (2020).
50. Y. Zhang, W. Zhang, P. Gao, X. Zhong, W. Pu, Finger-palm synergistic soft gripper for dynamic capture via energy harvesting and dissipation. *Nat. Commun.* **13**, 7700 (2022).

Acknowledgments
Funding: This work was supported by the UK Engineering and Physical Sciences Research Council (EPSRC) research grants EP/R02961X/1, EP/T020792/1, EP/V026518/1, EP/S026096/1, EP/V062158/1, and EP/R02961X/1 and the Royal Academy of Engineering Chair in Emerging

Technologies grant CIET1718/22. **Author contributions:** Conceptualization: T.Y., H.B.-G., and J.R. Methodology: T.Y., K.T., Q.Q., Z.L., and J.R. Software: T.Y. and K.T. Validation: T.Y. and C.L. Formal analysis: T.Y., C.L., and L.Y.L. Investigation: T.Y., C.L., L.Y.L., and J.R. Resources: T.Y., C.L., L.Y.L., and J.R. Visualization: T.Y. and J.R. Funding acquisition: J.R. Project administration: J.R. Supervision: H.B.-G. and J.R. Writing—original draft: T.Y. and J.R. Writing—review and editing: T.Y. and J.R. **Competing interests:** The authors declare that they have no competing interests. **Data and materials availability:** All data supporting this work are available at the University of Bristol data repository, data.bris, at https://doi.org/10.5523/bris.1dfontkssi562be7vf30jpyou, or within the main text and the Supplementary Materials.

Submitted 30 June 2024
Accepted 15 April 2025
Published 14 May 2025
10.1126/scirobotics.adr4264

Science Robotics

Embodying soft robots with octopus-inspired hierarchical suction intelligence

Tianqi Yue, Chenghua Lu, Kailuan Tang, Qiukai Qi, Zhenyu Lu, Loong Yi Lee, Hermes Bloomfield-Gad#lha, and Jonathan Rossiter

Sci. Robot. **10** (102), eadr4264. DOI: 10.1126/scirobotics.adr4264

Science Robotics (ISSN 2470-9476) is published by the American Association for the Advancement of Science. 1200 New York Avenue NW, Washington, DC 20005. The title *Science Robotics* is a registered trademark of AAAS.